

# TURBULENT BOUNDARY-LAYER SEPARATION

*Roger L. Simpson*

Department of Aerospace and Ocean Engineering, Virginia Polytechnic Institute and State University, Blacksburg, Virginia 24061

## 1. INTRODUCTION

This article summarizes our present understanding of the physical behavior of two-dimensional turbulent separated flows, which occur due to adverse pressure gradients around streamlined and bluff bodies. The physical behavior of turbulence is flow dependent, so detailed experimental information is needed for understanding such flows and modeling their physics for calculation methods. An earlier review (Simpson 1985) discussed in much detail prior experimental and computational work, and this was followed by an updated review of calculation methods only (Simpson 1987). Here additional recent references are added to those cited in the two other works.

By *separation*, we mean the entire process of *departure* or *breakaway*, or the breakdown of boundary-layer flow. An abrupt thickening of the rotational-flow region next to a wall and significant values of the normal-to-wall velocity component must accompany breakaway, or otherwise this region would not have any significant interaction with the free-stream flow. This unwanted interaction causes a reduction in the performance of the flow device of interest (e.g. a loss of lift on an airfoil or a loss of pressure rise in a diffuser).

It is too narrow a view to use vanishing surface shearing stress or flow reversal as the criterion for separation. Only in steady two-dimensional flow do these conditions usually accompany separation. In unsteady two-dimensional flow the surface shear stress can change sign with flow reversal without the occurrence of breakaway. Conversely, the breakdown of the boundary-layer concept can occur before any flow reversal is encountered. In three-dimensional flow the rotational layer can depart without the

surface shear stress necessarily falling to zero, and the wall shear is zero only at the singular points.

For steady free-stream two-dimensional flows on streamlined surfaces, separation begins intermittently at a given location; that is, the flow reversal at that location occurs only a fraction of the total time. At progressively farther downstream locations, the fraction of time that the flow moves downstream is progressively less.

For steady free-stream separating turbulent boundary layers, the following set of quantitative definitions on the detachment state near the wall has been proposed, with the definitions based on the fraction of time that the flow moves downstream,  $\gamma_{pu}$  (Simpson 1981): *Incipient detachment* (ID) occurs with instantaneous backflow 1% of the time ( $\gamma_{pu} = 0.99$ ); *intermittent transitory detachment* (ITD) occurs with instantaneous backflow 20% of the time ( $\gamma_{pu} = 0.80$ ); *transitory detachment* (TD) occurs with instantaneous backflow 50% of the time ( $\gamma_{pu} = 0.50$ ); and *detachment* (D) occurs where the time-averaged wall shearing stress  $\bar{\tau}_w$  is 0. Available data indicate that TD and D occur at the same location.

*Incipient detachment* has been observed experimentally when flow markers such as a dye filament injected into liquids at the wall or a tuft mounted on the surface occasionally move upstream. In the past this location has been called incipient separation. (Here we do not use the latter term, since it appears to have been used loosely to mean a flow near conditions required for the separation process to occur. In some cases, such as in supersonic flow, the separation process occurred but was not documented; it was often called incipient separation.) The zone just downstream of incipient detachment is important, since the displacement thickness of the boundary layer begins to increase rapidly there.

*Intermittent transitory detachment* has been observed in experiments when tufts or dye filaments moved upstream a noticeably greater fraction of the time than “occasionally.” Sandborn & Kline (1961) indicated that this location corresponds to the location of “turbulent separation” or “intermittent separation.” Sandborn (1970) labeled the velocity profile at this position as “unrelaxed.” *Transitory detachment* and *detachment* correspond to the same location if the streamwise velocity probability distribution at that location is symmetric. *Detachment* was called the location of “steady” separation by Sandborn & Kline, while Sandborn (1970) noted that the velocity profile at this location is “relaxed.” Until recently, many workers were concerned only with calculating the location of D, ignoring the fact that the turbulent-separation process starts upstream of this location in all but singular cases where ID and D are at the same location.

The length of the region between the ID, ITD, TD, and D points will

depend on the geometry and the flow, but the definitions of these points are the same (Figure 1*b*).  $\gamma_{pu}$  is not a sufficient variable to describe the flow behavior, since it only represents the fraction of a streamwise velocity probability distribution that is positive. However, it is important that such a feature be documented in all future work. In the next section flows on low-curvature streamlined surfaces are discussed, while later sections deal with surface-pressure fluctuations, wall-curvature effects, flows separating from sharp-edged bluff bodies, and unsteady effects.

## 2. STEADY FREE-STREAM SEPARATING TURBULENT BOUNDARY LAYERS

For low-curvature and flat surfaces, the mean flow upstream of ID obeys the “law of the wall” and the “law of the wake” as long as the maximum shearing stress  $-\rho\bar{u}w_{max}$  is less than  $1.5\tau_w$ . When  $-\rho\bar{u}w_{max} > 1.5\tau_w$ , the Perry & Schofield (1973) mean-velocity profile correlation, the law of the wall, and the Ludwig-Tillman skin-friction equation apply upstream of ITD. The qualitative turbulence structure is not markedly different from the zero-pressure-gradient case, except that the maximum fluctuations are in the middle of the boundary layer. The “bursting” frequency  $n$  of the

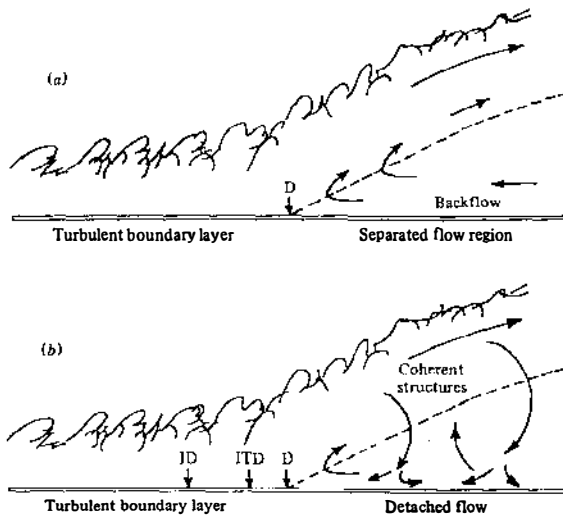


Figure 1 (a) Traditional view of turbulent boundary-layer separation with the mean backflow coming from far downstream. The dashed line indicates  $U = 0$  locations. (b) A flow model with the turbulent structures supplying the small mean backflow. ID, incipient detachment; ITD, intermittent transitory detachment; D, detachment. The dashed line denotes  $U = 0$  locations.

most energetic eddies near the wall is correlated by  $U_e/n\delta = 10$ , where  $U_e$  is the mean velocity outside the boundary layer and  $\delta$  is the boundary-layer thickness (Simpson et al. 1977).

Sandborn & Kline (1961) observed that a family of power-law-type mean-velocity profiles seemed to fit data near where appreciable intermittent backflow was observed. This family of profiles yielded the relation

$$h = \frac{H-1}{H} = \left(2 - \frac{\delta^*}{\delta_{0.995}}\right)^{-1} \tag{1}$$

among the velocity profile shape factor  $H = \delta^*/\theta$ , displacement thickness  $\delta^*$ , momentum thickness  $\theta$ , and boundary-layer thickness  $\delta$  at the  $0.995u_e$  velocity location. This relation is shown in Figure 2. Data (Simpson 1985) indicate that this closely describes the location of ITD. The mean wall

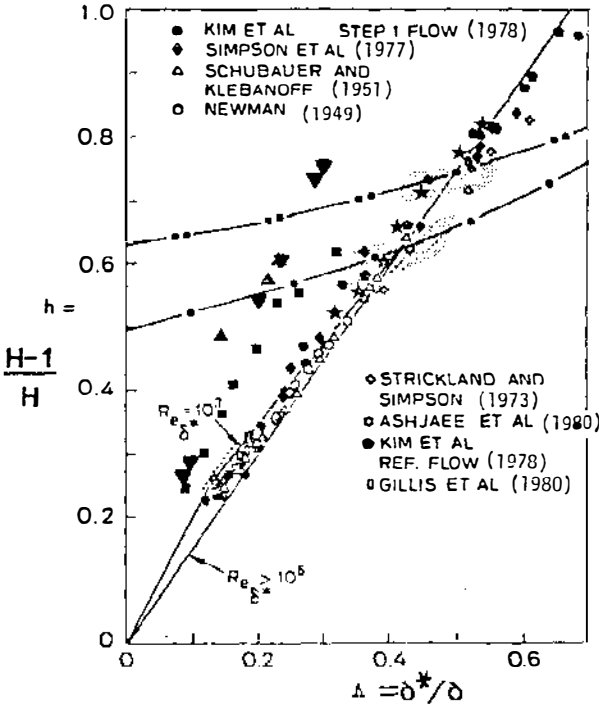


Figure 2 A plot of  $h$  vs.  $\delta^*/\delta$  data for detaching and reattaching flows (from Simpson 1985). Shaded regions—data reviewed by Sandborn & Kline (1961):  $\cdots$ , detachment;  $-\cdots-$ , intermittent transitory detachment. Curved wall data:  $\blacksquare$ , data of Chou & Sandborn (1973);  $\blacktriangle$ , data of Sandborn & Liu (1968);  $\star$ , data of Wadcock (1980);  $\dots$ , data of So & Mellor (1972) (zero pressure gradient);  $\blacktriangledown$ , data of Gersten et al. (1983).

shearing stress is greater than zero at this condition. Another family of power-law mean-velocity profiles that had zero shearing stress at the wall were used to describe conditions of detachment [Equation (6) of Sandborn & Kline]. Figure 2 shows this  $h$  vs.  $\delta^*/\delta$  relation at turbulent detachment, which also correlates laminar detachment data. The shaded regions on this figure show the data used by Sandborn & Kline and Kline et al. (1983) that support these relationships.

Figure 2 also shows  $h$  vs.  $\delta^*/\delta$  paths taken by several backward-facing-step reattaching and adverse-pressure-gradient-induced detaching flows. Using a modified Coles law-of-the-wall and law-of-the-wake mean-velocity profile model, Kline et al. showed that the  $h$  vs.  $\delta^*/\delta$  path is only weakly Reynolds number dependent even for low  $\delta^*/\delta$  and is nearly the same for flows on flat or low-curvature surfaces. The Perry & Schofield correlation produces a path among these data, as do the experiments of Chu & Young (1975). This path can be approximated by

$$h = 1.5(\delta^*/\delta) \quad (2)$$

for high Reynolds numbers. Note that it crosses the  $h$  vs.  $\delta^*/\delta$  relationships for intermittent backflow and detachment in the shaded regions. For near-equilibrium flows satisfying the Coles velocity profile model, intermittent transitory detachment occurs at  $\delta^*/\delta = 0.42$  and  $H = 2.70$ .

As a turbulent boundary layer undergoes an adverse pressure gradient, the flow near the wall decelerates until some backflow first occurs at incipient detachment. A spanwise line of detachment does not move up- and downstream as a unit. Small three-dimensional elements of flow move upstream for a distance and are later carried downstream. These reversed flows occur in regions of low kinetic energy and are caused by forces arising from the large-scale structures and adverse pressure gradient. Large eddies, which bring outer-region momentum toward the wall, supply some downstream flow. These large eddies grow rapidly in all directions and agglomerate with one another to decrease the average frequency of passage as detachment is approached. Substantial pressure-gradient relief begins near intermittent transitory detachment as the detaching shear layer grows at a rate proportional to  $\delta^2$ .

These large-scale structures supply the turbulence energy to the near-wall detaching flow. The velocity fluctuations in the backflow region are greater than or at least comparable to the mean backflow velocities. Intermittent backflow occurs as far away from the wall as the maximum shearing-stress location  $y/\delta \gtrsim \frac{1}{2}$ . Since the free-stream flow is observed to be rather steady, this means that the near-wall fluctuations are not mainly due to a flapping of the entire shear layer, but rather to turbulence within the detached flow. In such a high-turbulence-level flow, mean streamlines

do not represent the average pathlines for elements of fluids (Figure 1b). Even though the outer-region mean-velocity profiles look like those for a free mixing layer as shown in Figure 3, the inner region is substantially different. Mean-velocity profiles and their shape factors are almost independent of momentum-thickness Reynolds number, strongly correlate on  $\gamma_{pu}$  near the wall, and strongly depend on local turbulence conditions.

The mean backflow appears to be just large enough to satisfy continuity requirements. The backflow mean velocity  $U$  scales on the maximum negative velocity  $U_N$  and its distance from the wall,  $N$ , which varies with the shear-layer thickness  $\delta$ . Downstream of detachment the mean backflow can be divided into three layers: a *viscous layer* nearest the wall that is dominated by the turbulent-flow unsteadiness but with little Reynolds shearing-stress effects; an intermediate layer with a semilogarithmic mean-velocity profile that seems to act as an *overlap region* between the viscous wall and outer regions; and the outer backflow region that is really part of the *large-scale outer-region flow*. No “law-of-the-wall” type of velocity profile based on a wall shearing stress is valid for the backflow when  $\gamma_{pu} > 0$  and  $-\bar{u}\bar{v} \approx 0$  in the backflow. For downstream of detachment ( $\gamma_{pu} < \frac{1}{2}$  near the wall), Simpson (1983) presented the equation

$$\frac{U}{|U_N|} = A \left( \frac{y}{N} - \ln \left| \frac{y}{N} \right| - 1 \right), \tag{3}$$

where  $A = 0.3$ . This equation describes for a number of data sets the velocity profile of the middle region of the mean backflow ( $0.02 < y/N < 1.0$ , where  $N/\delta \lesssim 0.06$ ). Farther away from the wall

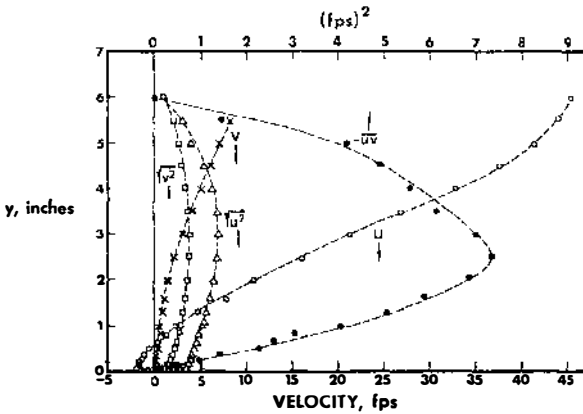


Figure 3 Mean-velocity and turbulence profiles downstream of detachment in the Simpson et al. (1981a) separating flow.

( $y/N > 1.0$ ) this equation does not describe the mean-velocity profile well, since this outer backflow region is influenced strongly by the large-scale outer-region flow. Nearer the wall ( $y/N < 0.02$ ), the viscous layer can be described by

$$\frac{U}{|U_N|} = -C\left(\frac{y}{N}\right) + \frac{P_1}{2}\left(\frac{y}{N}\right)^2, \quad \text{where } P_1 = \frac{N^2}{\rho\nu|U_N|} \frac{dP}{dx}, \quad (4)$$

and  $C$  is a constant. For this flow  $P_1 < 125$  and the pressure-gradient term contributes little. Here  $|U_N|/U_c$  varies almost linearly with  $1/H$ , being 0.15 at  $H = 10$ , where  $H$  is the mean-velocity profile shape factor  $\delta^*/\theta$  (Simpson & Shivaprasad 1983). Buckles et al. (1984) indicate that their backflow profiles agree with Equation (3). Dianat & Castro (1986) also report that Equation (3) fits their data, but with  $A = 0.235$ . They also suggest that a backflow skin-friction equation

$$\frac{\tau_w}{\frac{1}{2}\rho U_N^2} \approx 4.5 \text{Re}_N^{-1/2}, \quad \text{where } \text{Re}_N = \frac{U_N(L_r - X)}{\nu}, \quad (5)$$

fits reattachment as well as detachment data from a number of investigators for  $10^3 < \text{Re}_N < 10^5$ . Here  $(L_r - X)$  is the distance upstream of the reattachment location ( $\gamma_{pu} = \frac{1}{2}$ ). The  $-\frac{1}{2}$  exponent suggests that the unsteady backflow “boundary layer” is similar to a viscous boundary layer. Patrick (1987) also proposed the form of Equation (5) but with a constant of 3.29.

The intermittently forward flow ( $\gamma_{pu} > 0$ ) in the mean-backflow region can be due to only two effects. Either high-momentum forward flow moves toward the wall or high-momentum turbulent motions away from the wall set up instantaneous streamwise pressure gradients that are impressed onto the low-momentum wall region to produce instants of forward flow. Both of these effects contribute to the turbulent diffusion of energy, which is consistent with the conclusion given by Simpson et al. (1981b) that turbulent diffusion and dissipation are the main terms in the backflow turbulence-energy balance. Space-time correlations in the backflow indicate  $y$  length scales of the order of  $\delta$  (Chehroudi & Simpson 1985).

As detachment is approached, the large eddies produce  $\overline{w^2} = \overline{v^2}$  away from the wall. As a large structure the order of  $\delta$  in height and width supplies fluid toward the wall in the separated region,  $v$  fluctuations decrease and are exactly zero at the wall. Because of continuity requirements, the fluid must be deflected and must contribute to  $u$  and  $w$  fluctuations. Thus rms fluctuations  $u'$  and  $w'$  are a little greater owing to this wall effect than they would be with large-scale structure effects alone. This explains why  $u'$  and  $w'$  distributions have the inflection points near the

wall. Semilogarithmic profiles of  $\overline{u^2}$  and  $\overline{w^2}$  between inflection points suggest an overlap region between inner and outer velocity and length scales. No plausible explanation of these data appears possible when elements of fluid in the mean backflow are required to come from far downstream (Figure 1a).

Even though  $-\overline{w}$  is relatively large in the outer region (Figure 3),  $-\overline{w}/\overline{u'v'}$  and  $-\overline{w}/\overline{q^2}$  ( $\overline{q^2} = \overline{u^2} + \overline{v^2} + \overline{w^2}$ ) decrease during the separation process and downstream. In the backflow region these correlations are close to zero. The Reynolds shearing stresses must be modeled by relating them to the turbulence structure and not to local mean-velocity gradients. The mean-velocity profiles in the backflow are a result of time-averaging the large turbulent fluctuations and are not related to the cause of the turbulence. The inertial subrange of velocity spectra of the outer-region forward flow scale on the maximum shear stress at a given streamwise location, as shown by Nagabushana et al. (1988). The most energetic frequencies  $f$  in the backflow occur in the range  $10 \lesssim U_e/\delta f \lesssim 50$ .

Normal-stress effects contribute significantly to the momentum and turbulence-energy equations. Negligible turbulence-energy production occurs in the backflow. Normal- and shear-stress production in the outer region supply turbulence energy in the backflow by turbulent diffusion. Movies of laser-illuminated smoke also have clearly revealed that the large-eddy structure supplies most of the near-wall backflow. Fluid elements of the small mean backflow do not come from far downstream, as suggested in Figure 1a; rather, they appear to be supplied intermittently by large-scale structures as they pass through the separated flow, as suggested by Figure 1b. Blockage of the backflow region far downstream of detachment does not seem to affect the detachment location (Simpson et al. 1981b).

The flow studied by Buckles et al. (1984) also supports this view. Visualization of separated flow using surface-injected dye streaks (Zilker & Hanratty 1979) showed the separated shear layer rolling up into vortices that fill the backflow zone. In contrast, if this region behaved as a free shear layer, we would expect instead to see more isolated eddy structures with a passive fluid in the reversed-flow zone separating the shear layer from the surface (Buckles et al. 1984). The photographs of Zilker showed columnar motions carrying dye between the surface and the shear layer. Some of the dye columns correspond to strong, intermittent downward motions.

The data of Buckles et al. (1984) suggest a qualitative picture of the flow in which shear-layer vortices send fluid downward toward the wall and entrain fluid from the reversed-flow region upward into the shear layer. Large, positive skewness values and large flatness values (Simpson et al. 1981b) in the reversed-flow region near the wall imply intermittent pulses



of forward-moving fluid, possibly associated with the passage of shear-layer vortices overhead. These observations led Buckles et al. to suggest that the detached shear flow was driven by a mechanism other than just the external pressure gradient.

Of course, this mechanism for supplying the backflow may be dominant only when the thickness of the backflow region is small as compared with the turbulent shear-layer thickness, as in the Simpson et al. (1981a) flow. Experiments (Fox & Kline 1962, Patrick 1987) on separation in wide-angle diffusers indicate that the mean backflow can come mainly from downstream when the thickness of the backflow region is comparable to the thickness of the forward flow, although even in this case  $\gamma_{pu} > 0$  in much of the backflow. Thus, some forward flow is supplied to the near-wall region by the large eddies, with direct intrushes of forward flow and/or instantaneous favorable pressure gradients imposed on the wall region by the large eddies.

### 3. SURFACE-PRESSURE FLUCTUATIONS

It is well known that much higher levels of acoustic noise and pressure fluctuations are produced by a separated flow as compared with an attached boundary layer. In incompressible flow the fluctuating pressure  $p$  is related to the velocity fluctuations by the Poisson equation  $\nabla^2 p = -\rho\sigma$ , where the source term  $\sigma$  is given in tensor notation by

$$\sigma = 2 \frac{\partial U_i}{\partial x_j} \frac{\partial u_j}{\partial x_i} + \frac{\partial^2}{\partial x_i \partial x_j} (u_i u_j - \overline{u_i u_j}), \tag{6}$$

where  $U_i$  and  $u_i$  are the mean and fluctuating velocity components in the  $x_i$  direction. The first term on the right-hand side of this equation represents the turbulence and mean-shear interaction, while the second term represents the turbulence-turbulence interaction. For a wall-bounded flow, if contributions from surface integrals are neglected, then the fluctuating pressure at a point  $\mathbf{X}$  on the wall is given by

$$p(\mathbf{X}) = \frac{\rho}{2\pi} \int_{V>0} \frac{\sigma(\mathbf{R}_s) dV(\mathbf{R}_s)}{(\mathbf{X} - \mathbf{R}_s)}, \tag{7}$$

where the volume  $V$  integration is at position  $\mathbf{R}_s$  over the entire half-space containing the flow. This equation indicates that while surface-pressure fluctuations are produced from sources in a large region of the flow, contributions from various sources drop off rapidly with their distance from the point under consideration. Although several attempts have been made to calculate  $p$  from Equation (7), it appears that such efforts suffer

from the lack of accurate information about the fluctuating velocity field within the boundary layer (Willmarth 1975). Consequently, the effects of adverse pressure gradients and separation on surface-pressure fluctuations from such calculations are uncertain and need confirmation by experimental data.

As measured by Buckles et al. (1984) the rms surface-pressure fluctuations  $p'$  increase at detachment to a maximum just downstream of reattachment ( $\gamma_{pu} = \frac{1}{2}$ ). These fluctuations are large, being of the same order as the local mean-pressure difference. This behavior is consistent with that of other detached reattaching flows, as reviewed by Mabey (1972). The maximum rms value near reattachment is too large to be explained entirely by wandering of the reattachment location. Rather, it appears to be influenced by wide variations of the velocity of the fluid impinging on the wall at reattachment. These unsteady motions may be a combination of the unsteadiness caused by the passage of large-scale structures and by unsteadiness associated with the location of the reattachment point fluctuating upstream and downstream, as discussed in Section 5 below.

As suggested by Mabey (1982), the pressure fluctuations scale on the maximum shearing stress  $\tau_M$  for detaching turbulent boundary layers. Simpson et al. (1987) suggest that  $\overline{p^2}/\tau_M^2$  is proportional to the ratio  $\alpha$  of a streamwise length scale to length scales in other directions. The integral-length scale data of Chehroudi & Simpson (1985) show that  $\alpha$  is about 2.5 for the Simpson et al. (1981a,b) flow, which is in agreement with the Schubauer & Klebanoff (1951) results for  $\alpha$  in their separating flow. Downstream of detachment  $\overline{p^2}$  continues to increase, although  $p'/\tau_M$  increases to detachment and then decreases downstream. This decrease appears to be because the pressure-fluctuation-producing motions move increasingly away from the wall downstream of detachment.

Both the turbulence and mean-shear interaction and the turbulence-turbulence interaction in the pressure-fluctuation source term [Equation (6)] are important for detached flows. Velocity fluctuations are as large as mean velocities in the backflow. Reynolds shear stresses and their gradients are large away from the wall. Thus, the largest pressure fluctuations are not at the wall in a detached flow, but rather they must be near the middle of the shear layer. These large pressure fluctuations strongly influence the near-wall flow. Equation (7) indicates that  $p(x)/\tau_M$  on the wall must decrease if the source  $\sigma$  moves away from the wall. The distance from the wall to the maximum shear location  $N$  increases rapidly downstream of detachment and inversely correlates with the decrease in  $p'/\tau_M$  (Simpson et al. 1987).

The spectra of Simpson et al. (1987) for  $\overline{p^2}$  substantially agree with those

of other investigations of strong adverse-pressure-gradient attached flows (Figure 4), which were reanalyzed and renormalized on  $\tau_M$  by Simpson et al. (1987). Their data define a  $\omega^{-0.7}$  variation in the  $0.01 < \omega\delta^*/U_\infty < 1$  range for the attached flow, where  $U_\infty$  is the mean velocity outside the boundary layer. At higher frequencies the pressure-fluctuation spectrum  $\Phi(\omega)$  varies with  $\omega^{-3}$ . Downstream of the beginning of intermittent backflow,  $\omega\Phi(\omega)$  has a peak value near  $\omega\delta^*/U_\infty \approx 0.8$  of 10 dB in the ordinate scale of Figure 4 and a  $\omega^{-2}$  range at higher frequencies. For lower frequencies,  $\omega\Phi(\omega)$  varies with  $\omega$  near the beginning of intermittent backflow; farther downstream this low-frequency range varies with  $\omega^{2.4}$ .

The coherence of the pressure-fluctuation-producing motions remains high in the streamwise direction upstream of incipient detachment but drops drastically with the beginning of intermittent backflow. The streamwise coherence level downstream of detachment looks much like that for the spanwise direction for attached flows. This indicates that even over small streamwise distances, the detached-flow pressure-fluctuation-producing turbulent motions do not retain the same structural features.

At low frequencies, both upstream and downstream of detachment,  $U_c$  celerity of the pressure fluctuations increases with increasing frequency until near  $\omega\delta^*/U_\infty = 0.5-1$ , as observed by Simpson et al. (1987) and Brooks & Hodgson (1981). Upstream of detachment,  $U_c$  decreases at

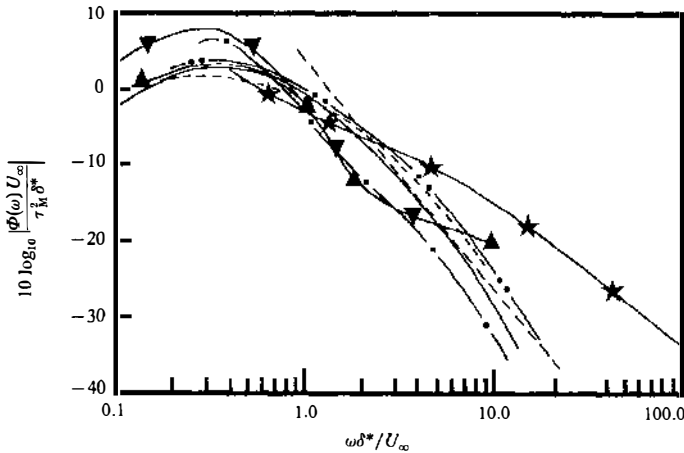


Figure 4 Surface-pressure-fluctuation spectra from some strong adverse-pressure-gradient turbulent boundary layers. Straight dashed line:  $\omega^{-3}$  variation. ---, Schloemer (1967)  $Re_{s^*} \times 10^{-4} = 1.46$ ; —, Bradshaw (1967)  $Re_{s^*} \times 10^{-4} = 4.0$ ; - · -, Burton (1973)  $Re_{s^*} \times 10^{-4} = 3.8$ ; · · · ·, Burton (1973)  $Re_{s^*} \times 10^{-4} = 2.4$ ; -★-, Lim (1971)  $Re_{s^*} \times 10^{-4} = 3.2$ ; -▲-, Panton & Linebarger (1974)  $Re_{s^*} \times 10^{-4} = 4.0, \alpha = 1$ ; -▼-, Panton & Linebarger (1974)  $Re_{s^*} \times 10^{-4} = 4.0, \alpha = 2$ . From Simpson et al. (1987).

higher frequencies and agrees asymptotically with the inner-outer overlap region equation given by Panton & Linebarger (1974). Downstream of the beginning of intermittent backflow, the instantaneous wave speed  $U_c$  can be both positive and negative for sufficiently high frequencies. Thus, the long-time-averaged  $U_c$  is lower than at upstream for these frequencies.

From the perspective of using pressure-fluctuation data to calculate far-field noise, one should probably locate the effective pressure-fluctuation sources along or near the locus of the maximum shear-stress position. The pressure-fluctuation-producing motions are concentrated in this region. The celerities of these fluid motions are probably close to those for the pressure fluctuations in this region.

This hypothesis is consistent with the idea of placing the effective pressure-fluctuation sources on the flow surface for low-pressure-gradient flows, since in these cases the maximum velocity gradients and shear stresses are at or very close to the wall. Since it is not possible to accurately measure pressure fluctuations within the turbulent separated flow, measurements of the far-field pressure fluctuation and the wall pressure fluctuation should be used to estimate the effective pressure fluctuations at the maximum-shearing-stress location.

#### 4. EFFECTS OF SURFACE CURVATURE

Convex or concave surface curvature ( $1/R$ ) without streamwise pressure gradients clearly influences the behavior of a turbulent boundary layer. Bradshaw (1973), Gillis & Johnston (1983), Barlow (1985), and Muck et al. (1986) reviewed the results from a number of experimental investigations in which  $\delta/R$  was as large as 0.1. Equations in curved-wall and in Cartesian coordinate systems apply (Bradshaw 1973). As pointed out by Wadcock (1980), the highly directional nature of the structure of a turbulent shear flow probably suggests that a mean streamline coordinate system be used so that familiar turbulence descriptions for low-curvature flows will apply approximately. In other words, since the turbulence structure is not invariant with coordinate-system rotation, the coordinate system following the flow should be used.

From experiments emerges an explanation of the effects of surface curvature on a flow. If the streamlines of the flow near the free stream in the turbulent-nonturbulent region have convex curvature, then  $\partial P/\partial n > 0$  and there is a reduction in entrainment downstream. This occurs because the tongues of large-eddy fluid that erupt into the free stream to engulf high-momentum fluid encounter an opposing pressure gradient that reduces their movement into the free stream. With a reduction in entrain-

ment, there are less mixing, lower Reynolds shearing stresses, lower triple-velocity correlations, and lower turbulence diffusion in the outer region. For concave curvature,  $\partial P/\partial n < 0$  and greater entrainment, mixing, and turbulent shearing stresses result.

In the above-mentioned experiments, the measurements were made in ducts where the streamwise pressure gradient was adjusted to zero. For flows over airfoils and blades, both convex surface curvature and adverse pressure gradients influence the detachment of a turbulent boundary layer. When an adverse pressure gradient is present, the outer-region streamlines are not curved as much as the convex surface, so there is less influence of curvature on entrainment than for a zero-pressure-gradient case. Baskaran et al. (1987) showed that convex curvature ( $\delta/R = 0.05$ ) reduces the momentum transport through a strong adverse-pressure-gradient turbulent boundary layer and causes detachment to occur farther upstream than for a comparable pressure-gradient flow without curvature.

For example, the data of Schubauer & Klebanoff (1951) showed little effect of surface curvature on the mean-velocity profile upstream of detachment, though  $\delta/R$  was 0.01 at the beginning of curvature and 0.024 near detachment. In fact, Perry & Schofield (1973) showed that these data fall within the scatter of data from flat-surface experiments, and that they obey their strong adverse-pressure-gradient velocity-profile correlations. The "zero-skin-friction" experiments of Stratford (1959) for flow over a short length of convex wall and a longer length of concave wall produced results also in close agreement with the Perry & Schofield correlations. Wadcock (1980) investigated with a flying hot-wire anemometer a separating turbulent boundary layer on the convex-curved surface of an NACA 4412 airfoil with  $\delta/R = 0.01$  upstream of detachment and  $\delta/R = 0.05$  near the trailing edge. These sets of data also agree with the flat surface  $h$  vs.  $\delta^*/\delta$  detachment criteria of Sandborn & Kline (1961; see Figure 2). The low-surface-curvature flow studied by Deutsch & Zierke (1986) shows little effect of curvature, and the  $h$  vs.  $\delta^*/\delta$  path follows that shown for zero-curvature surfaces in Figure 2. Wadcock's data showed no reduction in turbulence activity in the outer region. The curvature effect in the streamwise momentum equation was relatively negligible, while the curvature effect in the normal-to-surface equation was significant.

When the curvature of the surface quickly changes, the outer-region streamlines do not curve as rapidly. Near such a convex surface the flow direction and magnitude change quickly as a result of a local increase in flow cross-sectional area and an increase in surface pressure. As observed by Baskaran et al (1987), an "internal" boundary layer near the surface occurs in such cases, as in the channel-flow data of Buckles et al. (1984) showing a distinct knee in the velocity profile or discontinuity in  $\partial U/\partial y$  as

the flow proceeds downstream. As in the flows studied by Sandborn & Liu (1968) ( $\delta/R = 0.13$ ) and Chou & Sandborn (1973) ( $\delta/R = 0.1$ ), velocities near the wall decrease rapidly, thus changing the velocity-profile shape and the  $h$  vs.  $\delta^*/\delta$  path of the flow in Figure 2 and causing detachment to occur at lower values of  $h$ . Sandborn & Liu indicate that  $\gamma_{pu} \approx 0.7$  at the location where Equation (1) is satisfied. Thus in the absence of other data, Equation (1) may not be very good for calculating the location of ITD for strongly curved flows.

The flying hot-wire anemometer data of Thompson & Whitelaw (1985) in Figure 5 and the data of Gersten et al. (1983) and Adair (1987) appear to show this effect of rapidly changing surface curvature. In the outer region of these cases, there is lower curvature of the streamlines than of the wall as well as lower turbulence and velocity gradients. Outside  $0.6\delta$ , the turbulent shear stress is negligible (Thompson & Whitelaw 1985, Adair 1987). Spatial correlations show a normal-to-wall integral length scale  $L_y \approx 0.4\delta$  in this intermittent turbulent-nonturbulent region. Nearer the diverging wall, larger velocity gradients occur with much larger shearing and normal stresses. As in the Simpson et al. (1981a,b) flow, Thompson & Whitelaw found that the outer extremities of flow reversals coincide with the location of maximum Reynolds shear stress. Spatial velocity correlations show a normal-to-wall integral length scale  $L_y \approx 0.2\delta$  around the maximum-shear-stress location, indicating that the large active stress-producing eddies are a smaller fraction of  $\delta$  than for the flat-wall case of Chehroudi & Simpson (1985). Cross-stream pressure gradients cannot be ignored, and the displacement thickness is not an adequate link between

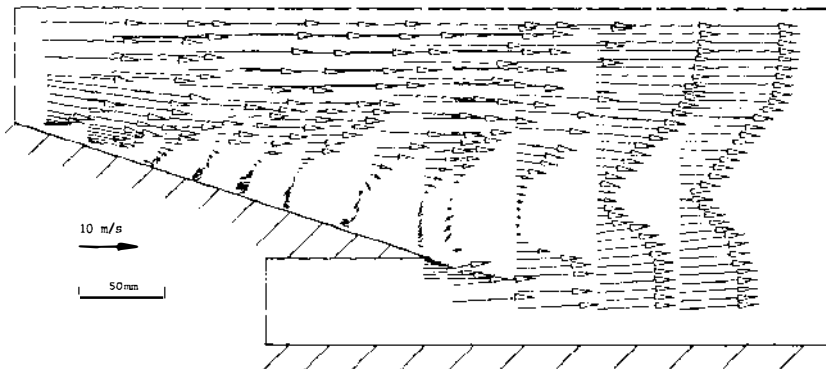


Figure 5 Mean-velocity vectors for the Thompson & Whitelaw (1985) trailing-edge separated flow.

viscous and inviscid regions, since normal-to-wall and streamwise terms of convection are of the same order of magnitude. As in the flat-wall case, mixing-length and eddy-viscosity models fail downstream of detachment in the backflow zone. Thompson & Whitelaw and Adair indicate that the backflow mean-velocity profile [Equation (3)] described by Simpson (1983) appears to hold downstream of detachment, indicating that the flow next to a diverging surface is little different from that on a flat surface. Minimum values of  $\gamma_{pu}$  and  $-\overline{uv}$  coincided in the backflow.

From these experiments and our understanding of the nature of separating turbulent boundary layers, we can summarize the qualitative effects of rapidly diverging surfaces on turbulent boundary layers. When a surface diverges from the local free-stream direction rapidly, mass-flow continuity requires that the near-wall velocity decrease more rapidly than would occur for a flat surface under the same streamwise pressure gradient. The available Reynolds shear stress and turbulence-energy diffusion are lower for a convex surface, so less momentum and energy are brought into the wall region to increase the velocity. Consequently, detachment occurs upstream of where it would occur under the same pressure gradient on a flat wall.

The lag of the turbulent flow in quickly responding to a diverging wall is due to the fact that the large energy-containing eddies do not respond instantaneously to rapid changes of boundary conditions (nonequilibrium condition). The Bradshaw et al. (1967) calculation method uses large-eddy turbulence-energy diffusion, which is related to the maximum turbulent shear stress and produces real characteristics from a hyperbolic set of equations (momentum, continuity, and turbulence energy). Real lags and upstream history effects can be calculated for separating turbulent boundary layers (Collins & Simpson 1978). Johnson & King (1985) showed also that large-eddy diffusion scaled on the local maximum turbulent shear stress accounted for the lag between the mean-flow and turbulence structure in separating turbulent boundary layers.

To define the effects of curvature clearly, complete data sets are needed. One problem with the available data that show an effect of convex surface curvature on separation is that no measurements of turbulence-energy diffusion were made. A second problem is the lack of Reynolds shearing-stress data; only Thompson & Whitelaw (1985) and Adair (1987) have measured that quantity. From Section 3 we know that the near-wall pressure and pressure-gradient fluctuations are closely related to the shear-stress-producing large eddies and influence the flow structure, and thus there is a need to measure and relate the surface-pressure fluctuation structure to the separated-flow structure in curved-wall flows. There are no such data currently available.

## 5. SEPARATION FROM TWO-DIMENSIONAL SHARP-EDGED BLUFF BODIES AND REATTACHMENT

The main obstacle to understanding this class of flows is that the major detachment occurs near the sharp edges of the body, with accompanying large variations in velocity and pressure around the detachment location. Here intermittent detachment is located very near detachment. The flow downstream of detachment is strongly dependent upon the upstream velocity distribution and the local geometry of the surface around the detachment location. Downstream of detachment, the thickness of the energetic outer-region flow is comparable in size to that of the backflow region. The zone of recirculating fluid is a substantial portion of the entire detached shear layer. At some distance downstream the turbulent shear layer reattaches to the surface or mixes with an adjacent stream in the near-wake.

Bluff-body, fence, rib, and forward-facing step data are discussed together because the mean-flow streamline at detachment from a sharp edge is at some large angle to the free-stream direction. For backward-facing step flows, the mean streamlines at detachment are almost parallel to the oncoming free-stream velocity direction. Cases with a thick initial boundary layer as compared with the step height are not discussed, since the oncoming turbulent boundary-layer structure is dominant and a bluff body on the surface acts as a roughness element.

### 5.1 *The Nature of the Backward-Facing Step Reattachment Flow*

Although the backward-facing step is the simplest reattaching flow, the flow field is still very complex. Figure 6 illustrates some of the complexities. The upstream boundary layer detaches at the sharp corner, forming a free-

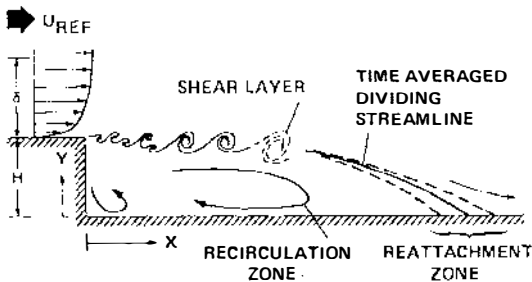


Figure 6 Features of a rearward-facing step flow (Driver et al. 1987).



shear layer. If the boundary layer is laminar, transition begins soon after detachment, unless the Reynolds number is very low.

The separated shear layer appears to be much like an ordinary plane-mixing layer through the first half of the separated-flow region. The dividing *mean*-flow streamline is only slightly curved, and the shear layer is thin enough that it is not affected by the presence of the wall (Figure 6). However, the reattaching shear layer differs from the plane-mixing layer in one important aspect: The flow on the low-speed side of the shear layer is highly turbulent, as opposed to the low-turbulence-level stream in a typical plane-mixing layer experiment.

The separated shear layer curves sharply downward in the reattachment zone and impinges on the wall, although any stabilizing effect of curvature appears to be small (Castro & Haque 1987). Part of the shear-layer fluid is deflected upstream into the recirculating flow by a strong adverse pressure gradient. The shear layer is subjected to the effects of adverse pressure gradient and strong interaction with the wall in the reattachment zone. A rapid decay of Reynolds normal and shear stresses occurs within the reattachment zone.

The recirculating flow region below the shear layer cannot be characterized as a dead-air zone. The maximum measured backflow velocity is usually over 20% of the free-stream velocity, and negative skin-friction coefficients as large as  $C_f = -0.0012$  (based on the free-stream velocity) have been measured (Adams & Johnston 1988).

Downstream of reattachment, the Reynolds stresses continue to decay rapidly for a distance of several step heights. Simultaneously, a new sub-boundary layer begins to grow up through the reattached shear layer. The measurements have shown that the outer part of the reattached shear layer still has most of the characteristics of a free-shear layer as much as 50 step heights downstream of reattachment. This observation demonstrates the persistence of the large-scale eddies that are developed in the separated free-shear layer.

This flow is highly unsteady. Large turbulent structures with length scales at least as large as the step height pass through the reattachment region. In addition, flow visualization showed that the length of the separation region fluctuated so that the instantaneous impingement location of the shear layer moved up and downstream. Quantitative measurements confirmed this conclusion and showed that the short-time-averaged reattachment location deviated from the long-time-averaged reattachment location by as much as  $\pm 2$  step heights. The nondimensional frequency of this motion is  $fX_R/U_0 \approx 0.6-0.8$ , which agrees with the results of Driver et al. (1987). Maximum energy content of wall pressure fluctuations occurs at these frequencies. Here  $X_R$  is the distance from the step to the long-

time-average location of reattachment, and  $U_0$  is the inviscid-flow velocity upstream of the step.

The period between flow reversals in the reattachment region appears to be random with no apparent correlation between the near-wall flow upstream and downstream of reattachment. Although the time  $T$  between flow reversals is such that  $X_R/TU_0 \approx 0.09$ , these flow reversals are short-lived during time  $t$ , with  $X_R/tU_0 \approx 0.6$  (Driver et al. 1987).

The largest structure in the flow originates from the roll-up and multiple pairing of spanwise vortices (Pronchick 1983). This roll-up is similar to the vortex roll-up and pairing process seen in the plane free-shear layer. The convective speed of these structures is about  $0.6U_0$ . The spanwise coherence or organization of these vortical structures starts to break down about 3 step heights downstream of detachment. The turbulence structure becomes fully three dimensional upstream of reattachment.

From their flow visualization studies, Muller & Gyr (1982) explained this breakdown behavior conceptually. As soon as a vortex tube is bent or distorted, it starts to induce velocities on itself (the Biot-Savart law). A vortex loop bent in the downstream direction moves away from the adjacent wall, while a vortex loop bent in the upstream direction moves closer toward the wall. The velocity induced on the near-wall vortex loop by its image vortex can cause it to move upstream relative to the surrounding flow, thus supplying some backflow and forming a very large streamwise length scale and a long time scale. The vortex tubes that are stretched in the streamwise direction lead to more intense mixing, greater Reynolds shearing stresses, and greater turbulence intensities.

Pronchick (1983) did not observe large-scale structures in the backflow zone. Instead, he found that the backflow consists of small-scale turbulent fluid created by eddy impingements on the wall and directed upstream by the adverse pressure gradient. This is not inconsistent with the conceptual description of Muller & Gyr (1982), which deals with the outer region upstream of reattachment.

The turbulence-intensity level of the detached flow is 5–10% higher than for the plane-mixing layers, which is believed to be the result of a very low frequency ( $fX_R/U_0 < 0.1$ ) vertical or “flapping” motion of the reattaching shear layer. Streamlines of the flow field at various times in a flapping sequence show that the amplitude of flapping is less than 20% of the shear-layer thickness, and that the flapping correlates with strong flow reversals in the vicinity of reattachment. There is a reduction in the reverse-flow rate with abnormally short instantaneous reattachment lengths. The shear stress in the flow increases dramatically with longer instantaneous reattachment lengths. Driver et al. (1987) suggest that the flapping is produced when a particularly high-momentum structure moves far down-

stream before reattaching. This would create a somewhat greater pressure gradient that would cause greater backflow at a later time. The flapping motion produces negligible contributions to the Reynolds shearing stress.

The distance from the step to the reattachment location  $X_R$ , where  $\gamma_{pu} \leq 0.5$  and  $C_f = 0$ , is an important length scale for normalizing the streamwise position in correlations of  $C_f$ ,  $\gamma_{pu}$ , surface pressure coefficient  $C_p$ , and pressure fluctuation data. The turbulent-flow reattachment length to step-height ratio  $X_R/H$  is mainly a function of the expansion ratio (downstream flow height/upstream flow height =  $h_2/h_1$ ) for step-height Reynolds numbers  $Re_H$  (based on the upstream free-stream velocity and the step height) above  $10^4$ . There is a strong Reynolds number dependence for  $Re_H < 6000$ . For  $h_2/h_1 > 2$ , there is little expansion-ratio dependence.  $X_R/H$  seems to increase with increasing initial-momentum-thickness Reynolds number and with increasing adverse pressure gradients. When the reattachment surface is divergent from the upstream flow,  $X_R/H$  increases. This is plausible, since the large-scale structures of the shear layer must travel farther in order to interact with the reattachment surface.  $X_R/H$  can be reduced by a curved edge on the backward-facing step.

Eaton & Johnston (1981) summarize other flow effects on reattachment length. High-free-stream-turbulence levels reduce the reattachment length, as do low-aspect-ratio test channels (width/step height  $< 10$ ). Rotation of the channel about a spanwise axis in the stabilizing direction reduces the three-dimensional turbulence and increases the reattachment length about 8% over the no-rotation case. Rotation in the opposite direction enhances the three-dimensional motions and decreases the reattachment length by 50%.

The maximum Reynolds shearing stress occurs near the maximum  $\partial U/\partial y$  value, as in detaching flows, and moves toward the wall as reattachment is approached. According to Pronchick's (1983) data, the shear correlation coefficient  $-\overline{uw}/u'v'$  is about 0.5 in the middle of the detached shear layer, decreasing toward the wall and the free stream. The data of Simpson et al. (1981a) for a detaching flow show a much lower value. Pressure fluctuations scale on the maximum shearing stress.

The mixing-length and eddy-viscosity ( $\epsilon_m/U_a\delta^*$ ) distributions for the detached flows of Driver & Seigmiller (1985) and Pronchick (1983) have maximum values of about one half those for an attached flow. This is in agreement with the results of Simpson et al. (1981a). The Reynolds-normal-stress terms of the momentum and turbulent-kinetic-energy equations appear to be important to these flows. Little diffusion of turbulence energy occurs in the backflow before the reattachment region is reached ( $\partial\gamma_{pu}/\partial x > 0$ ). In the backflow as reattachment is approached, the turbulence energy is supplied by diffusion and is balanced by dissipation,

since the production and advection terms are negligible. This behavior is consistent with that for detaching flows.

This type of detached flow can be manipulated by imposed unsteadiness. McGuinness (1978) and Roos & Kegelman (1986, 1987) modified the roll-up and pairing process by introducing periodic disturbances in the detached flow at frequencies characteristic of the passing of vortex structures, which resulted in shortened reattachment lengths. Like Roos & Kegelman, Reisenhelt et al. (1985) used an oscillating flap of length  $h$  at the backstep. At low reduced frequencies ( $k = fh/U_0 = 0.01\text{--}0.05$ ) and small flap extensions ( $45^\circ$ ), the flap does not generate much vorticity but periodically blocks the accumulation of vortical fluid at the backstep. This causes the shear-layer vortices to be drawn closer to the plate, thus shortening the reattachment length. At  $k = 0.06\text{--}0.09$  and a full flap extension ( $90^\circ$ ), the flap tip produces significant vorticity that merges with the shear layer to reduce  $X_R$  by 50%. Beyond  $k = 0.1$  with a full flap extension, the flap vortices are so close together that they do not allow the separated flow to reattach until they have diffused downstream, which produces a larger  $X_R$ .

Mullin et al. (1980) reported that M. Lebouché & M. Martin pulsed the oncoming mean flow. For  $fX_R/U_0 < 0.5$  the recirculation zone appeared to wash out periodically. For  $fX_R/U_0 > 0.5$  this zone appeared stable but smaller than for the steady free-stream case. In their own experiment, Mullin et al. used a sinusoidal oscillation with an amplitude 12% of the average and  $fX_R/U_0 \approx 0.04$ . The stall zone was washed out periodically at the time that the free-stream velocity reached its minimum.

### 5.2 *The Nature of Fence, Rib, and Forward-Facing Step Flows*

Figure 7 shows an instantaneous view of a uniform free-stream flow normal to a plate with a long splitter plate. The splitter plate eliminates the periodic vortex shedding from the two edges of the normal plate that occurs when

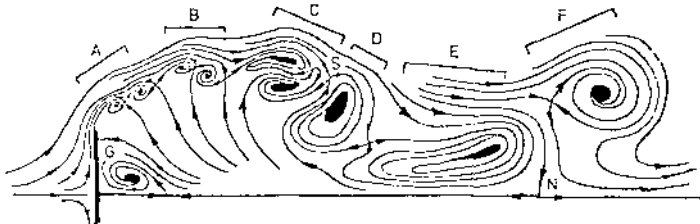


Figure 7 Instantaneous streamlines for flow over a bluff plate with a splitter plate (Smits 1982).

the normal plate is used alone. According to Smits (1982), after an initial Kelvin-Helmholtz-like roll-up of the vortex sheet, the vortices are seen to pair, triple, and even quadruple together. This process results in lower energy-containing frequencies in the downstream direction (Cherry et al. 1984). This appears to be the mechanism for the rapid growth of the shear layer and bears many similarities to the structure of a simple mixing layer. The structure that results from a number of vortices joining together appears to behave like a single vortex. The three dimensionality of the structures increases downstream, but the essential features of the flow, even near reattachment, are still recognizable.

Only vortex pairing is shown in Figure 7 for simplicity. Because of the high velocity gradient, small differences in the initial conditions of vortex pair A cause them to come together as in pair B. They commence to rotate around each other and deform in response to strains caused by their induced velocity (pair C). Viscosity smears out the vorticity, and the pair then acts like a single vortex (vortex D). Two pairs (C and D) begin to roll around each other, which forces the saddle point closer to the splitter plate. S becomes the instantaneous reattachment point, or saddle point, N. Vortex E enters the separation bubble while F proceeds downstream. Although E becomes highly distorted, stretched, and eventually entrained in the shear layer, there appears to be no vortex splitting. Note that all vortices are shown as foci—that is, flow goes into the vortices, which means that they are three dimensional. In the secondary separation bubble G, the fluid is transported laterally and expelled into the flow at the junction of the side wall and the splitter plate, and a complex eigenvalue critical point is observed at that point. Ruderich & Fernholz (1986) observed the same behavior.

As in the backward-facing step case, there is a significant low-frequency flapping of the shear layer near detachment and a modulation of shedding characteristics near reattachment. For other such sharp leading-edge geometries (Simpson 1985), low-frequency fluctuations are present with a characteristic time scale in which the shear-layer disturbances convect several reattachment lengths. Flow-visualization studies show that vorticity is shed from the recirculating flow as a series of more-or-less discrete turbulent structures with streamwise spacings of the order of  $0.6\text{--}0.8X_R$ . Between the shedding of successive structures, there was a noticeably thinner shear layer downstream of reattachment. This suggests that the low-frequency motions perhaps correspond to the period between shedding phases.

When there is an incident boundary layer on a fence, rib, or forward-facing step, the first detachment occurs upstream of the bluff body as a result of the adverse pressure gradient induced by the bluff obstacle.

Reattachment occurs on the front of the obstacle. For sharp-edged bodies the second detachment is located at the leading edge with the second reattachment on the obstacle if it is long enough. For short bodies the second reattachment occurs far downstream, while for long bodies a third detachment occurs with a backward-facing step type of flow. In either case, the downstream region of recirculation contains two vortices of opposite sense, as in the backward-facing step and splitter-plate flows.

The large-scale structures of the incident boundary layer are accelerated as they move over the leading edge of an obstacle, increasing the energy-containing frequencies and possibly subdividing the large-scale structures. Downstream of the flow acceleration, the energy-containing frequencies decrease because of the pairing process, described above for the splitter-plate flow and for the backward-facing step flow. Data indicate that  $f_{\max} X_R / U_\infty$  varies from about 7 to 10 near detachment to near 1 at reattachment, where  $f_{\max}$  is the peak energy-containing frequency of  $fF(f)$  vs.  $\log |f|$  of the  $u$  energy spectrum  $F(f)$ . For many cases, the spanwise spatial correlations at reattachment are the same when normalized on the vorticity thickness and are independent of Reynolds number.

Increasing the blockage of the obstacle in a flow channel increases the acceleration of the flow over the obstacle, leading to increased velocity gradients, turbulent mixing, and entrainment of fluid in the separated zone back into the shear layer. This in turn causes reattachment to occur farther upstream than if less blockage were present. As in the backward-facing step case, the reattachment length is the streamwise length scale for describing the reattaching flow.

The reattachment length varies with the flow angle  $\theta$  at detachment. Simpson (1985) showed that for a given blockage-area ratio, the non-dimensional reattachment length  $X_R/H = X'$  can be crudely approximated by

$$\frac{X'(\theta) - X'(0^\circ)}{X'(90^\circ) - X'(0^\circ)} = \sin \theta, \quad (8)$$

where  $X'(0^\circ)$  is from the backward-facing step case, and  $X'(90^\circ)$  is from the splitter-plate flow shown in Figure 7.

The reattachment length can be used as the streamwise length scale to normalize the streamwise distributions of  $C_p$ ,  $C_r$ , and  $\gamma_{pu}$  and to describe the behavior of velocity-profile distributions (Simpson 1985). The structure of these flows is qualitatively very close to that for a backward-facing step, although there are detailed quantitative differences (Castro & Haque 1987). The maximum shearing stress is the proper scale for the turbulence and pressure-fluctuation structure. The low-frequency flapping motion does not contribute to significant Reynolds-stress-producing motions.

Nakamura & Ozono (1987) found that for a blunt leading edge, the effect of the free-stream turbulence is to shorten the separation bubble with increasing intensity. For small-scale turbulence there is little effect of scale on the mean pressure distribution, as found by Hillier & Cherry (1981), but for larger scales the mean pressure distribution asymptotically approaches the smooth-flow distribution. In other words, very large-scale turbulence is equivalent to a flow with slowly fluctuating velocity, so that it can no longer influence the mean flow effectively.

## 6. UNSTEADY EFFECTS ON SEPARATION

While all turbulent flows are inherently unsteady, the term “unsteady” as used here means an organized time-dependent motion in contrast to the relatively aperiodic motion of turbulence. Periodic flow is by far the most common organized time-dependent motion. Two types are possible: one in which a periodic flow condition is imposed on a turbulent boundary layer, and a second in which the turbulent flow interacts with adjacent flow regions to set up a quasi-periodic motion. Here we summarize the physical behavior, with most references and details given in Simpson (1985). Reynolds & Carr (1985) reviewed unsteady separated flows driven by imposed flow oscillations.

Section 6.1 discusses experiments on unsteady separating turbulent flows on flat or low-curvature walls with imposed periodic inviscid free-stream velocity and pressure oscillations. Dynamic stall on helicopter and compressor blades is an example of the first type of periodic condition imposed on the boundary layer, and this topic is described in Section 6.2. Self-induced quasi-periodic motion has been observed under some conditions in diffuser, airfoil, and duct flows including shock-induced separation and is discussed in Section 6.3.

### 6.1 *Unsteady Separating Turbulent Boundary Layers*

Unsteady turbulent boundary layers are governed by the same equations as for the steady case, except that time-dependent effects must also be included. The difficulty of solving these equations is the same as that for steady flows, namely describing the behavior of the Reynolds shear stress  $-\overline{u'v'}$  for a given phase of an oscillation cycle. A number of investigators have argued that as long as the period of the organized unsteadiness is relatively long compared with the turbulence time scales, it should be acceptable to use the approximation that the turbulence structure is unaffected by the unsteadiness. Quasi-steady flow exists when the phase-averaged flow can be described by the steady free-stream flow structure. For moderate-amplitude oscillations (velocity amplitude/mean velocity =

$\tilde{U}/\bar{U} < 0.37$ ),  $-\widehat{uw}/\widehat{u\dot{w}}$  is independent of phase angle and has values corresponding to steady turbulent boundary layers, which thus confirms this argument. All low-frequency unsteadiness, moderate-amplitude attached-flow measurements indicate that outside of the near-wall region the turbulence structure is basically unaffected by organized unsteadiness.

When the frequency of the organized unsteadiness is comparable to energy-containing turbulence frequencies, this approximation may not hold. Substantial interaction between the periodic unsteadiness and the aperiodic turbulence may occur in this case, although the time-varying nearly random phase differences between these two kinds of motion at the same frequency suggest that there will be little effect on ensemble-averaged quantities.

Several experiments on strong adverse-pressure-gradient unsteady turbulent boundary layers with moderate-amplitude oscillations indicate that the outer region of ensemble-averaged velocity profiles look like the strong adverse-pressure-gradient steady turbulent boundary layers observed by Perry & Schofield (1973). A semilogarithmic velocity-profile region exists with a constant phase angle. Competing influences of the oscillating pressure gradient, Reynolds shearing stress, and inertia determine the phase shift of oscillating profiles within the boundary layer. For example, if the flow nearest the wall is governed by viscosity and the oscillating and mean pressure gradients such as near separation, then the solution to the unsteady vorticity equation

$$\frac{\partial \omega_z}{\partial t} = \nu \frac{\partial^2 \omega_z}{\partial y^2} \quad (9)$$

indicates that the near-wall velocity oscillation leads the pressure-gradient oscillation by  $135^\circ$ .

In some cases (e.g. Jayaraman et al. 1982), ensemble-averaged backflow is observed near the wall, although the mean velocities are not negative and a semilogarithmic region exists farther from the wall. One should not think of such a periodically reversed flow as detached, since no breakaway, as discussed in Section 1, was observed. In these cases, the imposed oscillatory pressure gradient dominated the low-momentum wall region and produced phase leads relative to the free stream that agreed approximately with the Stokes solution to Equation (9).

After the beginning of adverse-pressure-gradient-induced detachment, large amplitude and phase variations develop through the flow, and the structure is not quasi-steady. Unsteady effects produce hysteresis in relationships between flow parameters. As the free-stream velocity during a cycle begins to increase, the fraction of time that the flow moves down-



stream,  $\hat{y}_{pu}$ , at a given phase of the cycle increases as backflow fluid is washed downstream. As the free-stream velocity nears the maximum value in a cycle, the increasingly adverse pressure gradient at downstream locations causes progressively greater near-wall backflow while  $\hat{y}_{pu}$  remains high at the upstream part of the detached flow. After the free-stream velocity begins to decelerate, the location where flow reversal begins moves upstream. This cycle is repeated as the free-stream velocity again increases.

Near the wall in the backflow region, the ensemble-averaged velocity leads the free-stream velocity by a large amount. The phase angle of the periodic backflow velocity is nearly independent of  $y$  near the wall. The ensemble-averaged backflow near the wall behaves like a quasi-steady flow when normalized on the maximum phase-averaged negative velocity  $\tilde{U}_N$  and its distance from the wall  $\hat{N}$ , when  $-\hat{w} \approx 0$  near the wall. The turbulence structure progressively lags the ensemble-averaged flow oscillation (Simpson 1985).

Oscillation amplitude strongly influences the detached-flow behavior. Mean-velocity profiles for a large-amplitude flow ( $\tilde{U}/\bar{U} > \frac{1}{2}$ ) are much different in shape than those of the lower amplitude sinusoidal cases, since large variations of the detached shear flow occur and the shapes of the ensemble-averaged profiles for each phase of the cycle are much different than those of the lower amplitude flows. Unlike the lower amplitude sinusoidal waveform flows, there is little variation of the phase angle through the detached shear layer. This does not mean that this detached flow is quasi-steady, because higher harmonics and nonlinear effects are important. The waveform and amplitude of the unsteadiness strongly influence the detached-flow behavior. In order to improve our understanding of unsteady detached flows, measurements of Reynolds stresses and the turbulence structure have been made for these cases (Agarwal & Simpson 1987, 1988a,b).

## 6.2 *Dynamic Stall*

Dynamic stall on helicopter and compressor blades is associated with unsteady gusts and rapid changes in the angle of attack. If the angle of attack of an airfoil or other lifting surface oscillates about the static stall angle, large hysteresis develops in the fluid-dynamic forces and moments (McCroskey 1982). The unsteady turbulent boundary layers cannot be ignored because there is considerable interaction between the boundary layer and the inviscid flow during the high-lift operating conditions of these devices. In such cases the relatively thick boundary layer on the suction side of the lifting body is near separation. At the maximum normal-force angle of attack, the boundary-layer flow on the front third of the chord abruptly separates, causing a catastrophic drop in the normal force.

The magnitude of the reversed flow near the surface increases as the large separation vortex forms and moves downstream.

### 6.3 *Self-Induced Unsteadiness in Separating Turbulent Flows*

In many detaching turbulent boundary layers, there are conditions when unsteadiness is induced throughout much of the flow field by the interacting inviscid and turbulent-flow regions, even when the approaching flow is steady. In Section 5.1, a self-induced low-frequency flapping of the detached shear layer for a backward-facing step was discussed. Flows with shock waves can induce unsteadiness, as can large transitory stall in a two-dimensional diffuser.

Transitory stalls in diffusers of included angle  $2\Theta$  between walls are large, pulsating detached-flow regions that occur primarily in relatively narrow passages of symmetric shape. A positive pressure gradient exists all along the surfaces in all known data. The peak pressure recovery is achieved at the lowest  $2\Theta$  angles in this regime. At peak pressure recovery, both side walls have a nonzero fraction of time with flow reversal, but with  $\gamma_{pu} > 1/2$  and no detachment. The overall pressure recovery starts to fall off with an increase of  $2\Theta$  as soon as a zone of strong reversed flow is found solely on one side wall (Ashjaee & Johnston 1980). Even for  $2\Theta > 24^\circ$ , we have  $\gamma_{pu} > 0.1$  on the stalled wall in the transitory-stall regime, which indicates intermittent backflow.

The flow first detaches near the end of the diffuser, forming a stall. The stalled region grows toward the diffuser throat with fluid from the diffuser exit. After sufficient growth the stall becomes unstable, is entrained by the mainstream flow, and is washed out of the diffuser. The sequence then repeats itself. S. J. Kline & J. P. Johnston (Simpson 1979) suggest that the positive  $dP/dx$  is essential in sustaining the transitory-stall fluctuating flow pattern. Smith & Kline (1974) have shown that the maximum unsteadiness occurs just before some fixed stall zone is observed. It is the most complex and the least predictable flow regime.

In transitory stall, the maximum unsteadiness occurs for angles between walls of  $2\Theta$  in the range  $20^\circ$  to  $24^\circ$ . Large-amplitude fluctuations can occur more or less periodically as detached flow washes in and out of the downstream end of the diffuser or as the stalled region grows and collapses in the lateral direction. Lyrio et al. (1981) summarized the experiments on the period between washouts of part of the stalled fluid. Transitory stall induces inlet-flow unsteadiness on an otherwise disturbance-free flow, with the greatest unsteadiness occurring for  $2\Theta$  between  $16^\circ$  and  $22^\circ$ . A periodic inlet disturbance induces only moderate changes in the exit unsteadiness and a substantial change in the size of the exit blockage.

As summarized by Simpson (1985), unsteadiness can develop because of shock-wave/boundary-layer interactions. For steady approach flow over a biconvex airfoil (Marvin et al. 1980) at Mach numbers of 0.7–0.8, periodic unsteadiness is present. During the initial portion of the cycle, the flow on the upper surface of the airfoil is attached and accelerating. As the speed increases, a series of compression waves strengthen and coalesce into a single shock wave that moves upstream. A thick shear layer develops downstream of the shock wave, and detachment occurs. As the shock wave approaches midchord, it weakens and the shear layer collapses and is convected downstream. On the other side of the airfoil, a similar sequence occurs 180° out of phase. Sajben et al. (1982) report similar self-induced shock-position oscillations for transonic diffuser flow. Meier (1975) discussed shock-separation-induced oscillations for transonic flow in a curved channel, over a symmetric airfoil at an angle of attack, and in a Laval nozzle with the same mechanism as discussed here for airfoil and diffuser flows.

## 7. CONCLUSIONS

In recent years, the experiments discussed here and in Simpson (1985) have revealed that the structure of separated turbulent flows is much different than for attached flows. The largest turbulent stresses occur in the middle of the separated shear layer and are mainly due to large-scale structures. Pressure fluctuations produced by these structures are relatively large and influence the low-velocity backflow zone. Since the backflow is reentrained into the outer-region flow, this indicates that there is significant interaction between the pressure and velocity fluctuations. Although there have been a few experimental studies of surface pressure fluctuations, this interaction still remains to be examined.

The effects of significant wall curvature are not well described quantitatively, although most separation cases occur on curved walls. The separation process is controlled by the transport of momentum and energy toward the wall. The rate at which the outer flow supplies energetic flow along a diverging wall over an increasing area determines the detachment location and the downstream behavior. With this in mind, we need to measure the turbulent transport of momentum and energy.

Imposed and self-induced unsteadiness strongly influence detached flows. Detachment from sharply diverging walls leads to large transitory stall in diffusers and flapping shear layers around bluff bodies. Large-scale motions produced in such cases do not contribute much to turbulent shear stresses but change the mean flow and produce low-frequency pressure fluctuations. This behavior makes such flows difficult to calculate.

Future research should address these unresolved issues. Calculation methods should be physically based (Simpson 1987).

#### ACKNOWLEDGMENTS

I appreciate the Army Research Office, Office of Naval Research, National Aeronautics and Space Administration, and the Air Force Office of Scientific Research for supporting my research during the last 18 years. Many former students and research associates were indispensable in this work.

#### Literature Cited

- Adair, D. 1987. Characteristics of a trailing flap flow with small separation. *Exp. Fluids* 5: 114-28
- Adams, E. W., Johnston, J. P. 1988. Flow structure in the near-wall zone of a turbulent separated flow. *AIAA Pap. No. 88-0610*
- Agarwal, N. K., Simpson, R. L. 1987. The structure of large amplitude unsteady separating turbulent boundary layers. *AIAA Pap. No. 87-0191*
- Agarwal, N. K., Simpson, R. L. 1988a. Experimental study of unsteady separating turbulent boundary layers. *Final Rep. AFOSR, Dep. Aerosp. Ocean Eng., Va. Polytech. Inst. State Univ., Blacksburg*
- Agarwal, N. K., Simpson, R. L. 1988b. Large amplitude unsteady separating turbulent boundary layers. Submitted for publication
- Ashjaee, J., Johnston, J. P. 1980. Straight walled two-dimensional diffusers—transitory stall and peak pressure recovery. *J. Fluids Eng.* 102: 275-82
- Barlow, R. S. 1985. *Structure of turbulent boundary layers on a concave surface*. PhD dissertation. Stanford Univ., Stanford, Calif.
- Baskaran, V., Smits, A. J., Joubert, P. N. 1987. A turbulent flow over a curved hill. Part 1. Growth of an internal boundary layer. *J. Fluid Mech.* 182: 47-83
- Bradshaw, P. 1967. "Inactive" motion and pressure fluctuations in turbulent boundary layers. *J. Fluid Mech.* 30: 241-58
- Bradshaw, P. 1973. Effects of streamline curvature on turbulent flow. *AGARDograph 169*
- Bradshaw, P., Ferriss, D. H., Atwell, N. P. 1967. Calculation of boundary-layer development using the turbulent energy equation. *J. Fluid Mech.* 28: 593-616
- Brooks, T. F., Hodgson, T. H. 1981. Trailing edge noise prediction from measured surface pressures. *J. Sound Vib.* 78: 69-117
- Buckles, J., Hanratty, T. J., Adrian, R. J. 1984. Turbulent flow over large-amplitude wavy surfaces. *J. Fluid Mech.* 140: 27-44
- Burton, T. E. 1973. Wall pressure fluctuations at smooth and rough surfaces under turbulent boundary layers with favorable and adverse pressure gradients. *Rep. 70208-9, Dept. Mech. Eng., Mass. Inst. Technol., Cambridge*
- Castro, I. P., Haque, A. 1987. The structure of a turbulent shear layer bounding a separation region. *J. Fluid Mech.* 179: 439-68
- Chehroudi, B., Simpson, R. L. 1985. Space-time results for a separating turbulent boundary layer using a rapidly scanning laser anemometer. *J. Fluid Mech.* 160: 77-92
- Cherry, N. J., Hillier, R., Latour, M. E. M. P. 1984. Unsteady measurements in a separated and reattaching flow. *J. Fluid Mech.* 144: 13-46
- Chou, F.-K., Sandborn, V. A. 1973. Prediction of the turbulent boundary layer separation. *Rep. NTIS AD-766845, Colo. State Univ., Ft. Collins*
- Chu, J., Young, A. D. 1975. Measurements in separating two-dimensional turbulent boundary-layers. *AGARD-CP-168, Pap. 13*
- Collins, M. A., Simpson, R. L. 1978. Flow-field prediction of separating turbulent shear layers. *AIAA J.* 16: 291-92
- Deutsch, S., Zierke, W. C. 1986. The measurement of boundary layers on a compressor blade in cascade at high positive incidence angle. *NASA CR 179491 (Part I), NASA CR 179492 (Part II)*
- Dianat, M., Castro, I. P. 1986. Measurements in separating boundary layers using pulsed wire anemometry. *ICAS-86-1.7.2, 15th Congr. Int. Council. Aerosp. Sci., London*
- Driver, D. M., Seegmiller, H. L. 1985. Features of a reattaching turbulent shear layer

- in divergent channel flow. *AIAA J.* 25: 163-71
- Driver, D. M., Seegmiller, H. L., Marvin, J. 1987. Time-dependent behavior of a reattaching shear layer. *AIAA J.* 25: 914-19
- Eaton, J. K., Johnston, J. P. 1981. A review of research on subsonic turbulent flow reattachment. *AIAA J.* 19: 1093-1100
- Fox, R. W., Kline, S. J. 1962. Flow regimes for curved subsonic diffusers. *J. Basic Eng.* 84: 303-12
- Gersten, K., Wauschkuhn, P., Pagendarm, H.-G. 1983. Untersuchungen von Strömungen mit Ablösungsgebieten endlicher Länge. *Rep. 100/1983*, Inst. Thermo- und Fluiddyn., Ruhr-Univ., Bochum, Fed. Rep. Germ.
- Gillis, J. C., Johnston, J. P. 1983. Turbulent boundary layer on a convex, curved surface. *J. Fluid Mech.* 135: 123-53
- Hillier, R., Cherry, N. J. 1981. The effects of stream turbulence on separation bubbles. *J. Wind Eng. Ind. Aerodyn.* 8: 49-58
- Jayaraman, R., Parikh, P., Reynolds, W. C. 1982. An experimental study of the dynamics of an unsteady turbulent boundary layer. *Rep. TF-18*, Dep. Mech. Eng., Stanford Univ., Stanford, Calif.
- Johnson, D. A., King, L. S. 1985. A mathematically simple turbulence closure model for attached and separated turbulent boundary layers. *AIAA J.* 23: 1684-92
- Kline, S. J., Bardina, J. G., Strawn, R. C. 1983. Correlation of the detachment of two-dimensional turbulent boundary layers. *AIAA J.* 21: 68-73
- Lim, K. B. 1971. *A study of pressure fluctuations in turbulent shear flows under the effects of mean pressure gradients*. PhD dissertation. Univ. Adelaide, Adelaide, Aust.
- Lyrjo, A. A., Ferziger, J. H., Kline, S. J. 1981. An integral method for the computation of steady and unsteady turbulent boundary layer flows, including the transitory stall regime in diffusers. *Rep. PD-23*, Thermosc. Div., Dep. Mech. Eng., Stanford Univ., Stanford, Calif.
- Mabey, D. G. 1972. Analysis and correlation of data on pressure fluctuations in separated flow. *J. Aircr.* 9: 642-45
- Mabey, D. G. 1982. Comment on "A review of research on subsonic turbulent flow attachment." *AIAA J.* 20: 1632
- Marvin, J. G., Levy, L. L. Jr., Seegmiller, H. L. 1980. On turbulence modeling for unsteady transonic flows. *AIAA J.* 18: 489-96
- McCroskey, W. J. 1982. Unsteady airfoils. *Ann. Rev. Fluid Mech.* 14: 285-311
- McGuinness, M. 1978. *Flow with a separation bubble—steady and unsteady aspects*. PhD dissertation. Univ. Cambridge, Cambridge, Engl.
- Meier, G. E. A. 1975. Shock-induced flow oscillations. *AGARD-CP-168*, Pap. 29
- Muck, K. C., Hoffman, P. H., Bradshaw, P. 1986. The effect of convex surface curvature on turbulent boundary layers. *J. Fluid Mech.* 161: 347-69
- Muller, A., Gyr, A. 1982. Visualization of the mixing layer behind dunes. *Proc. Euro-mech 156, Mechanics of Sediment-Transport, Istanbul*
- Mullin, T., Greated, C. A., Grant, I. 1980. Pulsating flow over a step. *Phys. Fluids* 24: 669-74
- Nagabushana, K. A., Agarwal, N. K., Simpson, R. L. 1988. Features of separating turbulent boundary layers. *AIAA Pap. No. 88-0616*
- Nakamura, Y., Ozono, S. 1987. The effects of turbulence on a separated and reattaching flow. *J. Fluid Mech.* 178: 477-90
- Panton, R. L., Linebarger, H. G. 1974. Wall pressure spectra calculations for equilibrium boundary layers. *J. Fluid Mech.* 65: 261-87
- Patrick, W. P. 1987. Flowfield measurements in a separated and reattached flat plate turbulent boundary layer. *NASA CR 4052*
- Perry, A. E., Schofield, W. H. 1973. Mean velocity and shear stress distributions in turbulent boundary layers. *Phys. Fluids* 16: 2068-74
- Pronchick, S. 1983. *Experimental investigation of the turbulent flow behind a backward facing step*. PhD dissertation. Stanford Univ., Stanford, Calif.
- Reisenthel, P. H., Nagib, H. M., Koga, D. J. 1985. Control of separated flows using forced unsteadiness. *AIAA Pap. No. 85-0555*
- Reynolds, W. C., Carr, L. W. 1985. Review of unsteady, driven, separated flows. *AIAA Pap. No. 85-0527*
- Roos, F. W., Kegelman, J. T. 1986. Control of coherent structures in reattaching laminar and turbulent shear layers. *AIAA J.* 24: 1956-63
- Roos, F. W., Kegelman, J. T. 1987. Evolving three-dimensionality in a reattaching two-dimensional turbulent shear layer. *AIAA Pap. No. 87-1210*
- Ruderich, R., Fernholz, H. H. 1986. An experimental investigation of a turbulent shear flow with separation, reverse flow, and reattachment. *J. Fluid Mech.* 163: 283-322
- Sajben, M., Bogar, T. B., Kroutil, J. C. 1982. Unsteady transonic flows in a two-dimensional diffuser. *AFOSR-TR-0622*
- Sandborn, V. A. 1970. Boundary layer separation

- aration and reattachment. *NASA-SP-304*, pp. 279-99
- Sandborn, V. A., Kline, S. J. 1961. Flow models in boundary-layer stall inception. *J. Basic Eng.* 83: 317-27
- Sandborn, V. A., Liu, C. Y. 1968. On turbulent boundary layer separation. *J. Fluid Mech.* 32: 293-304
- Schloemer, H. H. 1967. Effects of pressure gradients on turbulent-boundary-layer wall-pressure fluctuations. *J. Acoust. Soc. Am.* 42: 93-113
- Schubauer, G. B., Klebanoff, P. S. 1951. Investigation of separation of the turbulent boundary layer. *NACA Rep. 1030*
- Simpson, R. L. 1979. Summary report on colloquium on flow separation. *Project SQUID Rep. SMU-3-PU*, Jet Propul. Cent., Purdue Univ., West Lafayette, Ind.
- Simpson, R. L. 1981. A review of some phenomena in turbulent flow separation. *J. Fluids Eng.* 102: 520-33
- Simpson, R. L. 1983. A model for the back-flow mean velocity profile. *AIAA J.* 21: 142-43
- Simpson, R. L. 1985. Two-dimensional turbulent separated flow. *AGARDograph* 287, Vol. 1
- Simpson, R. L. 1987. A review of two-dimensional turbulent separated flow calculation methods. *IUTAM Symp. Boundary Layer Separation, London, 1986*, ed. F. T. Smith, S. N. Brown, pp. 179-96. Berlin: Springer-Verlag
- Simpson, R. L., Shivaprasad, B. G. 1983. The structure of a separating turbulent boundary layer. V. Frequency effects on periodic unsteady freestream flows. *J. Fluid Mech.* 131: 319-39
- Simpson, R. L., Strickland, J. H., Barr, P. W. 1977. Failures of a separating turbulent boundary layer in the vicinity of separation. *J. Fluid Mech.* 79: 553-94
- Simpson, R. L., Chew, Y.-T., Shivaprasad, B. G. 1981a. The structure of a separating turbulent boundary layer. Part I. Mean flow and Reynolds stresses. *J. Fluid Mech.* 113: 23-51
- Simpson, R. L., Chew, Y.-T., Shivaprasad, B. G. 1981b. The structure of a separating turbulent boundary layer. Part II. Higher order turbulence results. *J. Fluid Mech.* 113: 53-73
- Simpson, R. L., Ghodbane, M., McGrath, B. E. 1987. Surface pressure fluctuations in a separating turbulent boundary layer. *J. Fluid Mech.* 177: 167-86
- Smith, C. R., Kline, S. J. 1974. An experimental investigation of the transitory stall regime in two-dimensional diffusers. *J. Fluids Eng.* 96: 11-15
- Smits, A. J. 1982. A visual study of a separation bubble. In *Flow Visualization II*, ed. W. Merzkirch, pp. 247-51. Washington, DC: Hemisphere
- So, R. M. S., Mellor, G. L. 1972. An experimental investigation of turbulent boundary layers along curved surfaces. *NASA CR 1940*
- Stratford, B. S. 1959. An experimental flow with zero skin friction throughout its region of pressure rise. *J. Fluid Mech.* 5: 17-35
- Thompson, B. E., Whitelaw, J. H. 1985. Characteristics of a trailing-edge flow with turbulent boundary-layer separation. *J. Fluid Mech.* 157: 305-26
- Wadcock, A. J. 1980. Simple turbulence models and their application to boundary layer separation. *NASA CR 3283*
- Willmarth, W. W. 1975. Pressure fluctuations beneath turbulent boundary layers. *Ann. Rev. Fluid Mech.* 7: 13-38
- Zilker, D. P., Hanratty, T. J. 1979. Influence of the amplitude of a solid wavy wall on a turbulent flow. Part II. Separated flows. *J. Fluid Mech.* 90: 257-71